PAPER

Check for updates

Mechanistic insights on ethanol dehydrogenation on Pd–Au model catalysts: a combined experimental and DFT study†

E. J. Evans Jr.,‡[a] H. Li,‡[b] Wen-Yueh Yu,[a] G. M. Mullen,[a] G. Henkelman [iD][b] and C. Buddie Mullins [iD]*[a]

In this study, we have combined ultra-high vacuum (UHV) experiments and density functional theory (DFT) calculations to investigate ethanol (EtOH) dehydrogenation on Pd–Au model catalysts. Using EtOH reactive molecular beam scattering (RMBS), EtOH temperature-programmed desorption (TPD), and DFT calculations, we show how different Pd ensemble sizes on Au(111) can affect the mechanism for EtOH dehydrogenation and H_2 production. The Au(111) surface with an initial coverage of 2 monolayers of Pd (2 ML Pd–Au) had the highest H_2 yield. However, the 1 ML Pd–Au catalyst showed the highest selectivity and stability, yielding appreciable amounts of only H_2 and acetaldehyde. Arrhenius plots of H_2 production confirm that the mechanisms for EtOH dehydrogenation differed between 1 and 2 ML Pd–Au, supporting the perceived difference in selectivity between the two surfaces. DFT calculations support this difference in mechanism, showing a dependence of the initial dehydrogenation selectivity of EtOH on the size of Pd ensemble. DFT binding energies and EtOH TPD confirm that EtOH has increasing surface affinity with increasing Pd ensemble size and Pd coverage, indicating that surfaces with more Pd are more likely to induce an EtOH reaction instead of desorb. Our theoretical results show that the synergistic influence of atomic ensemble and electronic effects on Pd/Au(111) can lead to different H_2 association energies and EtOH dehydrogenation capacities at different Pd ensembles. These results provide mechanistic insights into ethanol's dehydrogenation interactions with different sites on the Pd–Au surface and can potentially aid in bimetallic catalyst design for applications such as fuel cells.

Introduction

Hydrogen is one of the most extensively used molecules in the world. A few notable uses of hydrogen include the syntheses of ammonia and methanol, the removal of sulfur and nitrogen compounds from petroleum, and as a fuel source for rocket engines and fuel cells.[1] Despite the benefits of hydrogen use to society, its primary production methods need improvements to become more environmentally-friendly. Currently, over 90% of hydrogen production comes from methane steam reforming,

drawing heavily from fossil fuels and nonrenewable resources, but other techniques are being developed.[2] Considering the finite available resources, other sustainable means of H_2 production should also be investigated. The most prominent alternative method of H_2 production is electrolysis of water *via* heterogeneous photocatalysis,[3] and there are hopes of using photobiological organisms in the future.[4] Another potential method for H_2 generation involves biomass-derived liquids such as ethanol. With increasing interest in solving environmental and energy problems and the development of resources from biomass, ethanol can be a major player in the hydrogen production process. Currently Nissan is working on fuel cell vehicle technology to use ethanol as a hydrogen source with hopes of commercializing in 2020. Considering its relatively low toxicity and that infrastructure is already in place for its distribution, ethanol is a great medium for hydrogen storage and can contribute to the world's environmental and energy problems.

Considerable work has been performed regarding reactions of ethanol with the hope of using it to produce hydrogen, energy, or longer-chain hydrocarbons. The efficiency, selectivity, and

[a] *McKetta Department of Chemical Engineering and Department of Chemistry, Center for Nano and Molecular Science and Technology, Texas Materials Institute, Center for Electrochemistry, and Institute for Computational Engineering and Sciences, University of Texas at Austin, Austin, Texas 78712-0231, USA. E-mail: mullins@che.utexas.edu*

[b] *Department of Chemistry, Institute for Computational and Engineering Sciences, Texas Materials Institute, The University of Texas at Austin, 105 E. 24th Street, Stop A5300, Austin, Texas 78712, USA*

† Electronic supplementary information (ESI) available. See DOI: 10.1039/c7cp05097f

‡ These authors contributed equally to this study.

activity of ethanol dehydrogenation catalysts are dependent on various aspects such as the support material, the active metal, the preparation method, and the reaction conditions among others. Ethanol reforming to produce hydrogen has been investigated on noble metals where mechanistic pathways have been influenced by numerous characteristics of the catalyst.[5–9] When comparing Rh, Pt, Ru, Ni, and Pd on various supports and conditions, Rh has consistently been the most active for H_2 production, largely due to Rh's ability to break the C–C bond.[10–12] Although the solid/liquid interface can behave drastically different from that of the solid/gas interface, certain general trends for alloyed materials may be present across the different phase interfaces. For application in direct alcohol fuel cells, Xu *et al.* showed that Pd is a very effective anode for the ethanol oxidation reaction in alkaline media, surpassing the performance of the notable Pt metal on oxides and carbon nanospheres.[13,14] To improve stability, Pd has been alloyed with Au and has been shown to not only have more stable electro-catalytic activity than pure Pd due to the anti-poisoning properties of Au,[15,16] but it can also produce higher specific activity for the Pd added to the anode.[15,17] Furthermore, the Guerbet reaction for converting primary and short-chain alcohols to secondary and long-chain alcohols has been well studied over various catalysts such as MgO, Al_2O_3, and CuO_x.[18] More specifically, ethanol conversion to butanol, initiated through ethanol partial dehydrogenation, has received much attention in pursuit of better fuel additives. In both fuel cells and reforming reactions, a better understanding is needed regarding the interactions of ethanol on catalytic surfaces in order to construct inexpensive, efficient catalysts.

Many surface studies have been conducted on Pd and Au in regards to ethanol reactions. More specifically, clean Au(111) has been shown to be inert for ethanol activity at 77 K but can oxidize ethanol to various products when atomic oxygen is on its surface.[19–21] Density functional theory (DFT) calculations have supported these conclusions and provided insight into how ethanol adsorbs on the Au(111) surface.[22,23] On pure Pd, both theoretical and experimental work has been conducted on ethanol's adsorption interactions[22,24,25] and decomposition mechanism on different facets.[26–29] On Pd–Au alloys, there are fewer surface science studies, although there is evidence that the size of the Pd ensembles on Au has influence on the mechanism of certain reactions. For example, the ensemble effect on Pd–Au catalysts has been seen for hydrogenation of aromatic hydrocarbons while also showing a resistance to poisoning from sulfur compounds.[30] To our knowledge, there has not been a surface science investigation on EtOH dehydrogenation on Pd–Au alloys and the role that different Pd ensembles can play in EtOH reactivity.

In this work, we investigate how the different Pd ensembles on Au(111) change the mechanism and production of H_2 from EtOH decomposition. We found that the largest H_2 production occurs on 2 ML Pd–Au catalysts, having Pd(111)-like ensembles with enough surface Au atoms to limit CO poisoning and carbon contamination. An Arrhenius analysis suggests a difference in mechanism for H_2 production between isolated Pd atoms,

represented by the 1 ML Pd–Au surface, and Pd ensembles, represented by the 2 ML Pd–Au surface. Also, we investigated the stability of EtOH dehydrogenation on different Pd–Au surfaces, seeing more stability at low Pd coverage due to the ability of Au to readily desorb intermediates as opposed to contaminating the surface. Additionally, results from DFT calculations are presented in support of our experiments, elucidating the atomic ensemble and electronic effects of Pd/Au(111) surface alloys. H_2 association, initial EtOH dehydrogenation selectivities, and binding energies of different EtOH-related species were calculated on Pd/Au(111) with varying Pd ensemble sizes. The results from this study show that the activity, stability, and mechanism of ethanol partial dehydrogenation is heavily dependent on the type of Pd ensembles and sites that occupy the Au(111) substrate and can be purposely adjusted for heterogeneous catalysis.

Methods

Experimental methods

Experiments for this study were conducted in a molecular beam scattering ultrahigh vacuum (UHV) apparatus with a base pressure of 1×10^{-10} Torr that has been described in detail previously.[31,32] Briefly, the apparatus is equipped with Auger electron spectroscopy (AES) for surface elemental identification and quadrupole mass spectrometry (QMS) for detection of gaseous species, in addition to a molecular beam source and a series of apertures aligned to the Au(111) single-crystal sample for molecular beam impingement. The Au(111) single-crystal sample, cut into a circular disk 11 mm in diameter and 1.5 mm thick, is mounted to a tantalum plate that can be resistively heated to 900 K with a DC power supply regulated by a proportional–integral–differential controller. The Au(111) sample is in thermal contact with a liquid nitrogen bath for cooling to a minimum temperature of 77 K, which is monitored with a K-type thermocouple (alumel–chromel) spot welded to the tantalum plate. For each Pd–Au catalyst, the gold surface was cleaned by Argon ion bombardment (2 keV) at room temperature, followed by annealing to 800 K for 15 minutes. Cleanliness was verified by AES with an electron beam energy of 3 keV and emission current of 1.5 mA.

Pd–Au model surfaces were prepared by depositing Pd atoms from a homemade thermal evaporator onto the Au(111) surface at 77 K and then annealing the surface to 500 K for 10 min under UHV conditions. The deposition rate of Pd was calibrated with a quartz crystal microbalance (QCM) controller by assuming that the thickness of 1 monolayer (ML) of Pd is equal to the diameter of a Pd atom (0.274 nm). For our experiments, the alloys of Pd and Au are denoted as Pd–Au, with the initial Pd coverage indicated as a number of monolayers. Previous work from Koel *et al.* leads us to believe that growth of the Pd overlayer on the Au(111) surface at 77 K obeys an epitaxial layer-by-layer mechanism,[33] limiting alloy formation until after annealing when the Pd atoms diffuse into the Au(111) subsurface.

In this study, we used reactive molecular beam scattering (RMBS) experiments (modified King and Wells measurements)

This journal is © the Owner Societies 2017

Phys. Chem. Chem. Phys., 2017, **19**, 30578–30589 | 30579

to observe H_2 production from EtOH dehydrogenation and acquire kinetic information on our Pd–Au catalysts. The EtOH-RMBS experiments were conducted by impinging EtOH on a stainless steel inert flag to establish a baseline signal, followed by impingement on the Pd–Au surface at a specified temperature while monitoring the reactants and products *via* QMS. The flux for all experiments was estimated to be about 3×10^{14} molecules per cm^2, which was determined by analyzing the EtOH coverages on clean Au(111) and assuming that 1 monolayer of EtOH is equal to the surface atom density of Au(111), 1.39×10^{15} molecules per cm^2 (most likely between 0.35×10^{15} molecules per cm^2 and 1.39×10^{15} molecules per cm^2 but the actual value is unknown). Furthermore, temperature-programmed desorption (TPD) was conducted by heating the Pd–Au sample at 1 K s^{-1} while monitoring the products and reactants with the QMS after EtOH exposure *via* the molecular beam. Unreacted reactants and products were monitored using the following QMS signals: EtOH ($m/z = 31$ and 45), Acetaldehyde ($m/z = 29$, 44, and 15), CO ($m/z = 28$), and H_2 ($m/z = 2$). To ensure determination of the proper product, QMS signals for other potential products were also investigated throughout both RMBS and TPD experiments: CO_2 ($m/z = 44$), formaldehyde ($m/z = 29$, 30), formic acid ($m/z = 29$, 46), methane ($m/z = 15$, 16), ethane ($m/z = 27$, 28), ethylene ($m/z = 26$, 27, 28), acetic acid ($m/z = 43$, 60), ethylene oxide ($m/z = 29$, 44, 15), methyl formate ($m/z = 60$), ethyl acetate ($m/z = 43$), ethyl formate ($m/z = 27$, 28, 29), and methyl acetate ($m/z = 43$, 74).

Computational methods

DFT calculations were performed with the Vienna Ab initio simulation package (VASP).[34] Core electrons were described within the projector augmented-wave framework.[35,36] For all calculations in this study, electron correlation was evaluated within the generalized gradient approximation (GGA) using the Perdew–Burke–Ernzerhof (PBE) functional.[37] For the valence electrons, Kohn–Sham wave functions were expanded in a plane wave basis set with the energy cutoff of 300 eV.[38,39] van der Waals correction (DFT-D3) in the VASP package was used for binding energy calculations.[40] The Brillouin zone was sampled with a $(3 \times 3 \times 1)$ Monkhorst–Pack k-point mesh and integrated using the method of Methfessel and Paxton.[41,42] Energy barriers were determined with the climbing image nudged elastic band (CINEB) method.[43] Geometries were considered optimized when the force on each atom fell below 0.05 eV Å^{-1}. Spin polarization was tested and used as needed. Zero-point energy (ZPE) calculations were tested on several metallic (111) surfaces and were found to have negligible influence on the binding energies of EtOH-related species and the H atom. Therefore, we did not include this correction in our study.

Although electrochemical deposition of Pd affects the Pd adsorption site,[44] thermal annealing of Pd on Au(111) results in alloyed (111) surfaces.[45,46] Therefore, all calculations were modeled on the slab(111) surface of a 4-layer, (4×4) unit cell, face-centered cubic (FCC) surface. For our DFT calculations, the Pd and Au alloys are denoted as Pd$_x$/Au(111), where x is the

number of Pd atoms in the ensemble on the Au(111) surface. All the Pd/Au(111) models in this study are the Au(111) slab models with Au atoms at the (111) surfaces replaced by varying numbers of Pd atoms, forming the (111) surfaces that contain both Pd and Au. The bottom two layers of the slab were fixed in bulk position while the first two layers were allowed to relax. Binding energies of absorbed molecules (except H binding energy) were calculated using eqn (1):

$$E_{\text{b}} = E_{\text{slab+molecule}} - E_{\text{slab}} - E_{\text{molecule}} \tag{1}$$

where $E_{\text{slab+molecule}}$ is the energy of the slab model with one adsorbed molecule, E_{slab} is the energy of the bare slab, and E_{molecule} is the energy of the molecule.

Using the H_2 molecule as the reference, the H binding energies $E_{n\text{H}}$ were calculated using eqn (2):

$$E_{n\text{H}} = E_{\text{slab}+n\text{H}} - E_{\text{slab}} - \frac{n}{2}E_{\text{H}_2} \tag{2}$$

where $E_{\text{slab}+n\text{H}}$ is the energy of the slab model with n adsorbed H atom, E_{slab} is the energy of the bare slab, and E_{H_2} is the energy of the H_2 molecule.

Results and discussion

Characterization of model catalyst

The four model catalysts constructed in this work consisted of Au(111) substrates with initial Pd coverages of 1 ML, 2 ML, 3 ML, and 4 ML Pd. After annealing for 10 minutes at 500 K, a Pd–Au alloy is formed as the Pd sinks into the Au(111) substrate as shown by Shih *et al.* using Auger electron spectroscopy (AES).[47] Additionally, Yi *et al.* confirmed Pd–Au alloying using low energy ion scattering spectroscopy in which Pd and Au were evaporated onto a Mo(110) substrate[48] and XPS confirmed that there is little to no Pd clustering on the Au(111) surface upon annealing at higher temperatures.[33,48] For this study, the AES spectra (Fig. S1, ESI†) and Pd (328 eV)/Au (69 eV) ratios (Table S1, ESI†) before and after annealing at 500 K for 10 minutes were taken for 1, 2, 3, and 4 ML Pd–Au catalysts, as shown in the ESI.† Considering that annealing temperature and time remain the same for all Pd–Au catalysts throughout this study, the relative quantities of Pd on the surface depend predominantly on the initial Pd coverage. The decrease in Pd/Au ratios from before annealing to after annealing indicate that Pd has diffused into the Au(111) surface, forming a Pd–Au alloy. Additionally, with larger Pd depositions, there are corresponding increases in Pd features and decreases in Au features. Both phenomena were previously seen in work investigating how annealing in different atmospheres affects the alloy structures of Pd–Au.[46]

Pd–Au model catalysts in which Pd is evaporated on Au(111) have been further characterized in previous works. Using H_2 and CO as probe molecules, Yu *et al.* showed that the resulting Pd–Au alloys contain Pd–Au interface sites, in which isolated Pd atoms are surrounded by Au atoms, and Pd(111)-like sites, in which adjacent Pd atoms form an island.[49] Temperature-programmed desorption (TPD) of H_2 on the four catalysts was used to determine the relative amount of Pd–Au interface sites
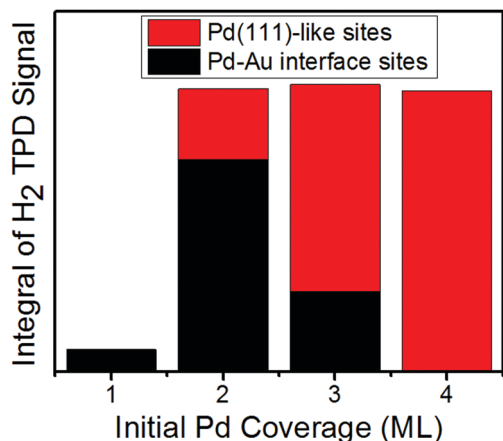
30580 | *Phys. Chem. Chem. Phys.*, 2017, **19**, 30578–30589

This journal is © the Owner Societies 2017

Fig. 1 Integrals of H_2 QMS signal intensity for H_2-TPD spectra of Pd–Au surfaces shown in Fig. S2 (ESI†) after peak deconvolution.

and Pd(111)-like sites, as shown in Fig. 1. The TPD spectra are displayed in Fig. S2 of the ESI.† At 1 ML Pd–Au, only the Pd–Au interface sites are present, shown by the H_2 desorption from 175 K to 300 K. However, upon increasing the Pd coverage from 2 to 4 ML, we observe H_2 desorption features that peak at 310 K. This indicates the presence of Pd island sites that become larger as Pd coverage increases, which is consistent with what was observed by Yu *et al.* on their Pd–Au catalysts.[50] Here, we see that the 4 ML Pd–Au surface has predominantly Pd(111)-like sites for H_2 desorption at about 310 K, matching the H_2 desorption peak of Pd(111)[51] and Pd–Au[49,52] seen in previous works and differing from the 360 K and 300 K desorption temperatures seen on Pd(100)[53] and Pd(110),[54] respectively. Therefore, we suspect the facet that is most prevalent on the Pd island sites on Pd–Au catalysts to be Pd(111)-like. Variation in relative quantities of Pd–Au and Pd(111)-like sites can play a significant role in the activity and stability of the catalytic production. In fact, Yu *et al.* saw how Pd–Au interface sites and Pd(111)-like sites have different selectivities towards dehydration and dehydrogenation of formic acid.[50] To further show the roles Pd active sites can play on Au(111), we investigate the mechanistic influences different Pd ensembles have on EtOH dehydrogenation and its effect on H_2 production.

Additionally, DFT calculations were used to further support the presence of different H binding sites using multiple Pd ensemble sizes as shown in Fig. S3 (ESI†). These ensembles were considered for DFT calculations in previous work by Yu *et al.* to investigate oxygen activation on Pd–Au catalysts.[45] Previously, we found that on Pd/Au alloy NPs, a triatomic ensemble (Au_3, Pd_1Au_2, Pd_2Au_1, or Pd_3) is the smallest unit that can adsorb H because it provides a 3-fold hollow site for H to occupy.[55,56] Therefore, the 3-fold triatomic ensembles of Pd_1Au_2 and Pd_2Au_1 are analogous to Pd–Au interface sites shown for 1 ML Pd–Au catalysts, while Pd_3 is analogous to Pd(111)-like sites. In Fig. S4 (ESI†), we calculated the binding energy of H atoms on different Pd ensembles on a Au(111) slab. The H binding energy gets stronger when going from Au_3 to Pd_3 triatomic ensembles on Au(111), as shown in Fig. S4 (ESI†).

As the Pd ensembles get larger than 3 atoms, the H binding energy has very little change. In Fig. S5 (ESI†), we calculated the binding energies of H atoms in the 3-fold ensembles of Pd/Au surface alloys, generated by randomly distributing Pd on Au(111), with varying Pd coverage. As Pd coverage is increased, Pd_3 sites become more prevalent with a corresponding increase in H binding energy. Similarly to the Pd–Au and Pd(111)-like quantities shown in Fig. 1 and the TPD data in Fig. S2 (ESI†), H_2 desorption from the Pd island sites appear upon higher initial Pd coverage. This H_2 desorption occurs at higher temperatures than that of the Pd–Au interface sites, indicating a stronger H binding energy. The DFT calculations support the characterization of Pd–Au interface and Pd(111)-like sites while showing the diversity of active sites for H_2 desorption.

H_2 production from the reaction of EtOH with varying Pd coverage

To investigate H_2 production on different Pd–Au surfaces, we evaporated initial Pd coverages of 1 ML, 2 ML, 3 ML, and 4 ML on Au(111). After annealing at 500 K for 10 minutes the Pd–Au alloy is ready for experimentation. A previous surface science study by Gong *et al.* showed that EtOH does not react measurably on the clean Au(111) catalyst.[21] Therefore, any H_2 production from EtOH on the Pd–Au surface is due to sites that involve Pd atoms. To quantify H_2 production, we performed EtOH reactive molecular beam scattering (RMBS) experiments, in which EtOH was impinged on a stainless steel inert flag from 10–15 s to serve as a baseline of no activity, followed by EtOH impingement on the Pd–Au sample from 60–65 s to observe H_2 production. In Fig. 2a, we see the production of H_2 from all four Pd–Au surfaces with the largest H_2 production from the 2 ML Pd–Au catalyst and the lowest from the 1 ML Pd–Au surface. Considering that the major difference between 1 ML and 2 ML Pd–Au is the appearance of Pd(111)-like sites, we attribute the increase in H_2 production to these sites. At even higher Pd coverages (3 ML and 4 ML Pd–Au), the amount of H_2 production decreases from that of 2 ML Pd–Au. This suggests that although the Pd(111)-like sites are responsible for the reactivity of the EtOH decomposition, additional amounts of Pd can result in more side reactions that decrease the amount of H_2 that can be readily formed.

Accompanying the H_2 production is acetaldehyde ($m/z = 29$) as shown in Fig. 2b. Acetaldehyde production from 3 ML and 4 ML Pd–Au are excluded in Fig. 2b for simplicity. EtOH (primary mass fragment of $m/z = 31$) also has a mass fragment that contributes to the $m/z = 29$ signal. Considering that EtOH does not react on Au(111),[21] we can use the $m/z = 29$ signal from EtOH King and Wells experiment on Au(111) as a baseline for acetaldehyde production, as seen in Fig. 2b. On 1 ML and 2 ML Pd–Au, there is a slight increase in the $m/z = 29$ signal, which we attribute to acetaldehyde production. This product is not seen in other UHV studies on Pd surfaces. Davis *et al.* saw the production of only CO, H_2, and CH_4 from ethanol TPD on clean Pd(111) surfaces.[29] Similarly, Shekhar *et al.* did not observe any acetaldehyde production on Pd(110) surfaces.[28] However, Davis *et al.* produced acetyl intermediates after EtOH

This journal is © the Owner Societies 2017

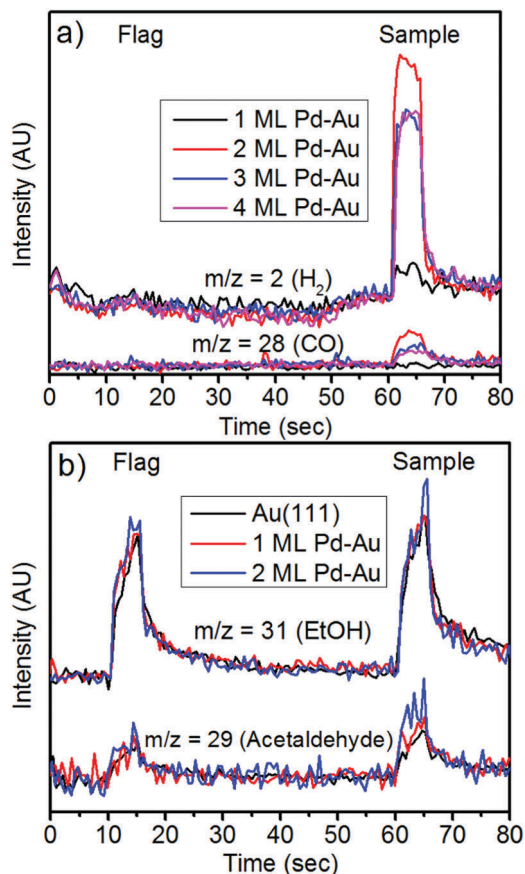*Phys. Chem. Chem. Phys.*, 2017, **19**, 30578–30589 | 30581

Fig. 2 (a) H_2 and CO production and (b) EtOH desorption and acetaldehyde production from modified King and Wells experiments of the decomposition of ethanol at 500 K on a Au(111) catalyst with varying initial Pd coverage. The EtOH molecular beam was impinged on the stainless steel inert flag from 10–15 s and on the Pd–Au surface from 60–65 s.

exposure on Pd(111) using HREELS, which further decompose to CO, H_2, and CH_4.[25] Alloying the inert Au with the active Pd may result in a more favorable environment for the acetyl intermediate to readily hydrogenate and desorb rather than decompose further. Additionally, in Fig. 2a, we see that there is no CO (m/z = 28) production for the 1 ML Pd–Au catalyst, whereas it is produced at higher Pd coverages (2 ML, 3 ML, and 4 ML Pd–Au). In addition to the drastic change in activity, there appears to be a distinction in selectivity when going from 1 ML Pd–Au to 2 ML Pd–Au with the 1 ML Pd–Au surface only showing measurable yields of acetaldehyde and H_2 from EtOH. Considering that there are both Pd–Au interface sites and Pd(111)-like sites, the heterogeneity of the Pd–Au catalysts may enable both EtOH dehydrogenation to acetaldehyde and decomposition to CO, H_2, and CH_4. Although the H_2 and acetaldehyde production is minor on the 1 ML Pd–Au surface compared to the other surfaces, the higher selectivity is worth noting. Processes that require highly selective partial dehydrogenation of alcohols to aldehydes such as Guerbet chemistry converting ethanol to acetaldehyde[57] may benefit from using less active material to tailor the active sites to yield the desired intermediate for further reactions downstream.

Although the overall trend of H_2 production shown in Fig. 2a is of primary importance for this study, we also calculated the turnover frequencies (TOF) for H_2 production similarly to that of Yu *et al.*[50] to obtain further insight on our catalysts (Table 1). Briefly, the TOF can be determined using the H_2 signal produced from EtOH dehydrogenation in the modified King and Wells experiment, H_{EtOH}, and the H_2 signal obtained from temperature-programmed desorption (TPD), H_{TPD}. The H_2 produced from the scattering experiments is divided by the time period of H_2 production. The number of Pd sites that H atoms can occupy are obtained from the area under the TPD curve multiplied times two because the molecule H_2 (not H atoms) is what is detected by the QMS. Dividing the H_2 produced over a period of time by the number of Pd sites provides the equation $TOF = \dfrac{H_{EtOH}/\Delta t}{H_{TPD} \times 2}$. The TOF depends on the flux of molecules impinging on the surface. Considering that this is a UHV study, the flux of our molecular beam is fairly small compared to the flux in practical systems, resulting in significantly smaller values. Despite the smaller values, TOF can provide an idea of the utilization of the Pd used on our Pd–Au model catalysts when comparing the values to each other.

From the calculated TOF for H_2 production, the 2 ML Pd–Au catalyst shows the most effective use of Pd atoms. This shows that not only does 2 ML Pd–Au have the highest H_2 production, but its sites are most effectively utilized for dehydrogenation of EtOH compared to the other three surfaces, offering the right combination of active Pd sites and the more inert Au where desorption can occur more readily. With that being said, the 1 ML Pd–Au catalyst has a significantly higher TOF than 3 and 4 ML Pd–Au model catalysts despite having less Pd, which is the active metal for EtOH activity. A potential reason for this disparity of H_2 production is a difference in selectivity towards dehydrogenation. For the 1 ML Pd–Au catalyst, only acetaldehyde and H_2 can be observed, indicating that side reactions that could diminish the Pd utility towards H_2 production are not prevalent. On the other hand, carbon contamination and side reactions that produce small hydrocarbons, as observed on pure Pd surfaces, can poison useful sites or incorporate H atoms into another reaction, resulting in a decrease of the TOF. These side reactions result in more consumption of EtOH, but less H_2 has been produced. Therefore, of the four Pd–Au surfaces, the 2 ML Pd–Au catalyst offers the best balance of selectivity to and activity of H_2 production while minimizing harmful side reactions (Table 1).

In addition to differences in reaction pathways, the heterogeneity on Pd–Au catalysts can also affect the ability for H atoms to recombine and desorb as H_2 from the Pd–Au catalyst.

Table 1 The turnover frequencies (H_2 produced/(H atom site $\times$ s)) for H_2 production at 500 K at varied Pd coverages on Au(111)

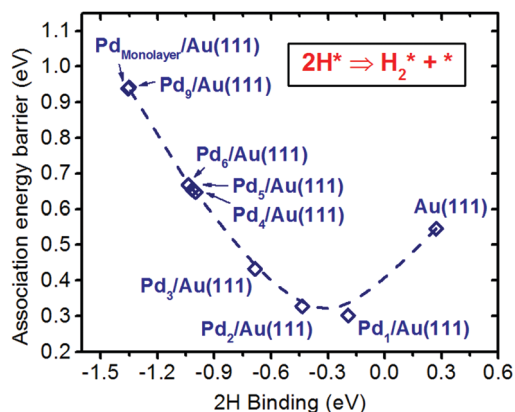| Pd coverage	TOF (H_2/(site $\times$ s))
1 ML Pd–Au	3.75×10^{-3}
2 ML Pd–Au	4.82×10^{-3}
3 ML Pd–Au	2.14×10^{-3}
4 ML Pd–Au	1.75×10^{-3}

Fig. 3 H_2 association energy barrier *vs.* H binding energy for Pd/Au(111) with varying Pd ensemble sizes. The Pd/Au(111) surfaces used for these calculations are shown in Fig. S3 (ESI†); the reaction pathway of H_2 association and desorption are shown in Fig. S6 (ESI†).

Based on the DFT and CINEB calculations, the rate-limiting step of H atoms recombining and desorbing as H_2 on Pd/Au(111) surfaces is H_2 association. To better understand the H_2 association barrier, we calculated the H_2 association and desorption energies on Pd/Au(111) surfaces of varying Pd ensemble sizes (Fig. S6, ESI†). Fig. 3 shows the H_2 association energy barrier *vs.* the binding energy of the co-adsorption of two H atoms on Pd/Au(111) surface alloys with varying Pd ensemble sizes. The co-adsorption of two H atoms takes into account the interactions between two H atoms in neighboring binding sites, which more closely resembles experimental H_2 association than simply using the binding energy of single H atoms. Contrary to the monotonic trend of the binding energy of two co-adsorbed H atoms, the H_2 association energy barrier has a parabolic shape as the Pd ensemble size increases with the smallest barrier for H recombination – and consequently, the most facile H_2 evolution – occurring on Pd–Au interface sites (Pd$_1$/Au(111) and Pd$_2$/Au(111)) and the barrier steadily increasing with Pd ensembles larger than 3 atoms. Although Au(111) has the weakest co-adsorbed H binding energies, its H_2 association energy barrier is higher than those of Pd$_1$, Pd$_2$, and Pd$_3$ ensembles because the pure Au(111) surface has a weaker driving force to recombine H atoms compared to surfaces with Pd ensembles. With that being said, surface diffusion of adsorbed H atoms plays a significant role in H_2 evolution. Takehiro *et al.* showed that surface diffusion on isolated Pd ensembles is hindered by the surrounding Au sites.[52] This inability to overcome surface diffusion on Au(111) could possibly affect the 1 ML Pd–Au production at lower temperatures considering that it only has isolated Pd atoms. On the other hand, the 2 ML Pd–Au catalyst would have fewer Au(111) areas and more Pd–Au interface sites that H atoms could readily navigate and recombine. Considering that the experiments shown in Fig. 2 were conducted at 500 K, above the H_2 desorption temperature from both Pd(111) and Au(111) surfaces, we do not suspect surface diffusion or the differences in association barrier to affect our results. However, these results provide insight for catalytic design of the desired sites to maximize H_2 recombination and subsequent desorption.

Although we used the binding energy of two co-adsorbed H atoms in Fig. 3, it is worth noting that our results also show that single H atom binding energies can be used as a reactivity descriptor for the H_2 association energy barrier on Pd/Au(111) alloys. Furthermore, the H binding energies calculated on random Pd/Au(111) surface alloys for the four triatomic ensembles (Au$_3$, Pd$_1$Au$_2$, Pd$_2$Au$_1$ and Pd$_3$) (Fig. S5a, ESI†) are quite close to those calculated at Au(111), Pd$_1$/Au(111), Pd$_2$/Au(111) and Pd$_3$/Au(111) sites (Fig. S4, ESI†), respectively. Therefore, whether the model involves a single H atom or two co-adsorbed H and a Pd ensemble on Au(111) slab or randomly dispersed Pd atoms throughout a Au(111) slab, we expect a similar parabolic trend of H_2 association energy *vs.* H binding energy.

Changing temperature showcases different mechanism

In Fig. 2, differences in product distributions for EtOH decomposition between 1 ML Pd–Au and 2 ML Pd–Au are shown. This indicates a difference in mechanism for EtOH dehydrogenation on these two surfaces with 1 ML Pd–Au containing predominantly isolated Pd sites and 2 ML Pd–Au containing some Pd island sites. To investigate the potential difference in mechanisms toward H_2 production, we created an Arrhenius plot by varying the temperature of the catalyst from 400 K to 500 K while impinging EtOH on the 1 ML and 2 ML Pd–Au surfaces. Arrhenius plots display the empirical relationship between reaction rate and temperature through the natural logarithm of the Arrhenius equation: $\ln(k) = -\dfrac{E_a}{RT} + \ln(A)$, where k is the reaction rate, E_a is the Arrhenius activation energy, R is the universal gas constant, T is temperature in Kelvin, and A is the pre-exponential factor. If there are differences in Arrhenius activation energies for H_2 production between 1 ML Pd–Au and 2 ML Pd–Au for H_2 production, it would suggest that the mechanism for that production differs. In Fig. S7 of the ESI,† we have the modified King and Wells experiments of EtOH on the (a) 1 ML and (b) 2 ML Pd–Au catalysts at temperatures ranging from 400 to 500 K in 25 K increments. The turnover frequencies for these experiments increased with increasing temperature and are provided in Table S2 of the ESI.†

The Arrhenius plots in Fig. 4 were constructed by integrating the area under the curve of the modified King and Wells experiments in Fig. S7 (ESI†), subtracting the H_2 signal upon impingement of EtOH on the inert flag from the H_2 signal produced from EtOH impingement on the catalyst. From the Arrhenius plots, we calculated Arrhenius activation energies of the two processes by determining the slope. For 1 ML Pd–Au and 2 ML Pd–Au, we obtain barriers of 13.9 kJ mol^{-1} and 10.7 kJ mol^{-1}, respectively, suggesting a difference in mechanisms for ethanol dehydrogenation of the two surfaces. Additionally, the fact that the activation barrier for 2 ML Pd–Au is lower than that of the 1 ML Pd–Au surface is consistent with the disparity in production. This is also supported by a higher pre-exponential factor for the 2 ML Pd–Au catalyst which was 6% higher than that of the 1 ML Pd–Au catalyst. With 1 ML Pd–Au containing predominantly isolated Pd atoms and 2 ML Pd–Au containing Pd(111)-like islands, the difference in mechanism is likely due to the
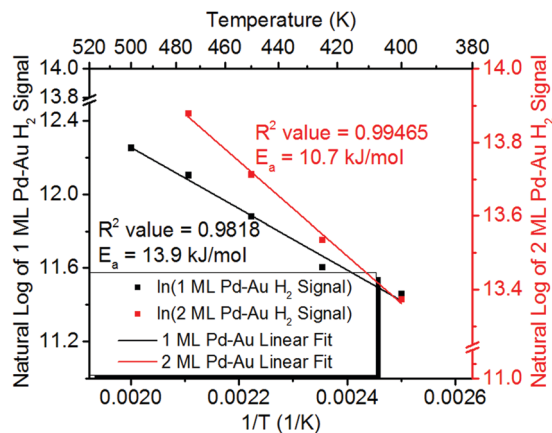
This journal is © the Owner Societies 2017

Phys. Chem. Chem. Phys., 2017, **19**, 30578–30589 | **30583**

Fig. 4 Arrhenius plots to determine the Arrhenius activation energy for H_2 production by using the integral area of the H_2 signal from EtOH dehydrogenation on 1 ML and 2 ML Pd–Au. The y-axis to the left is for 1 ML Pd–Au, and the y-axis to the right is for 2 ML Pd–Au.

Fig. 5 (a) Binding configurations of EtOH on Pd_x/Au(111), (x = 1, 4 and 9). (b) Activation energy barrier for three different dehydrogenation processes on Pd_x/Au(111), (x = 1, 4 and 9).

orientation of Pd atoms on the surfaces, providing different Pd sites for EtOH dehydrogenation.

It should be noted that the H_2 production from the modified King and Wells experiment conducted at 500 K on the 2 ML Pd–Au catalyst has been excluded from determining the Arrhenius activation energy. For determining the Arrhenius activation energy of EtOH dehydrogenation, it is essential for the mechanism to remain the same for the temperature range of the reaction. At 500 K, CO produced from EtOH reactions on 2 ML Pd–Au can readily desorb from the catalytic surface without occupying sites necessary for dehydrogenation. On the other hand, some adsorbed CO remains on the surface at temperatures below 475 K, considering that it desorbs in a range from 400 K to 490 K, peaking at 465 K. This is shown in Fig. S8 in the ESI,† where EtOH decomposition is conducted at 400 K and 425 K on the 2 ML Pd–Au catalyst. Therefore, the higher temperature of 500 K is excluded from the determination Arrhenius activation energy of the 2 ML Pd–Au catalyst because sites for EtOH dehydrogenation are not blocked by CO at higher temperatures as they are at 400 K to 475 K. Furthermore, Yu *et al.* showed that CO and H_2 compete for the same sites.[58] Therefore, CO may not only prevent EtOH dehydrogenation but also may hinder the recombinative desorption of H_2 from those occupied sites, reinforcing a difference in mechanism between the two temperature regimes. CO poisoning is a large hindrance on reactions on many catalysts, notably on fuel cell operation. In work done by He *et al.*, it was shown that Pd_4Au/C, having dominant facets of Au(111) and Pd(111), had a higher resistance to CO poisoning than Pt/C and Pd_3Sn/C while maintaining reasonable ethanol oxidation activity, showing how Au can help resist CO poisoning.[16] The increases in our activity may not be due to Au, but its low affinity for binding molecules can enhance CO-poisoning tolerance, resulting in more efficient catalysts.

DFT calculations on initial dehydrogenation of EtOH

To support our observations from the modified King and Wells experiments and provide insight at the molecular level, we conducted DFT calculations of the initial step of EtOH dehydrogenation
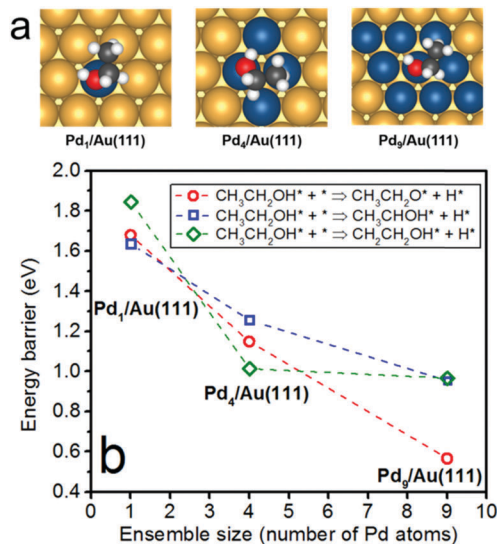
for different Pd ensembles. Fig. 5 shows the calculated activation energy barriers of three potential initial dehydrogenation steps (O–H bond, α-carbon–H, or β-carbon–H) for Pd_x (x = 1, 4, and 9) ensembles on a Au(111) slab. Due to the high computational overhead, we only examined the first dehydrogenation steps in this study, with the assumption that the first dehydrogenation steps would significantly influence the following decomposition mechanism.[59] Illustrations of the first dehydrogenation step and their corresponding activation barriers are shown in Fig. S9–S11 (ESI†). As the Pd ensemble gets larger, the activation barrier for dehydrogenation decreases for each mechanism, reinforcing the fact that reactivity is due to Pd atoms and showing a general Pd ensemble effect on EtOH dehydrogenation. However, no clear trend is apparent regarding which reaction pathway is most favorable. For the Pd_1 ensemble, α-carbon dehydrogenation has the lowest activation barrier at 1.63 eV, followed by hydroxyl dehydrogenation at 1.68 eV. This pathway indicates that acetyl species or alkoxide might be readily formed, which is similar to what was reported previously on Pd(111).[25,28] However, with the less active Au on the surface, desorption will more readily occur instead of further dehydrogenation or decomposition, favoring acetaldehyde production as seen in Fig. 2b. For Pd_4 ensembles, the lowest energy barrier for the initial step of EtOH dehydrogenation is observed at the β-carbon. This mechanism can lead to surface-bound carbon formation, which can contaminate the catalytic surface and reduce further activity for the desired reaction. There is additional discussion regarding carbon contamination later in this paper.

For Pd_9 ensembles on Au(111), we see a significant decrease in the energy barrier of hydroxyl dehydrogenation to 0.57 eV. Alkoxide formation is consistent with most experimental work done on EtOH reactions, including Pd(111), so this result is not surprising. Despite the drastic change in the activation barrier for alkoxide formation between the Pd_4 and Pd_9 ensembles, there is very little change for α- or β-carbon dehydrogenation.

A plausible explanation is that there are Pd electronic effects shown for hydroxyl dehydrogenation, but it is less influential for α- and β-carbon dehydrogenation. For Pd, both atomic ensemble effects[60–63] and electronic effects[63,64] have been seen for other reactions under various conditions. Considering the heterogeneity of the Pd–Au catalyst, it is not surprising that we see both of these effects for EtOH dehydrogenation. It should be noted that the DFT-calculated energy barriers (Fig. 5) should not be directly compared to the experimental activation energies (Fig. 4). On both 1 ML and 2 ML Pd–Au surfaces, there should exist Pd ensembles of varying sizes, and the experimental activation energies incorporate all of the ensembles on the catalytic surface. The target mission of Fig. 5 is to show the general trends for tuning the EtOH dehydrogenation capacity and selectivity with varying sizes of Pd ensembles on Au(111), not a direct comparison of numerical values.

Incorporating the results of H_2 association (Fig. 3) with that of the different dehydrogenation mechanisms (Fig. 5), we observe a synergistic effect of Pd/Au(111) from a computational perspective. We see from Fig. 3 that smaller Pd ensembles (Pd_1/Au(111) and Pd_2/Au(111)) offer the lowest energy barrier for H_2 recombination. However, larger Pd ensembles provide the smallest activation energy barriers for EtOH dehydrogenation. Therefore, compositions of Pd and Au that offer a balance of Pd/Au interface sites and Pd island sites may enable sufficient EtOH dehydrogenation while H atoms can recombine and desorb efficiently. Based on our experiments, this may qualitatively explain why the 2 ML Pd–Au catalyst yielded the largest production of H_2 compared to other initial Pd coverages (Fig. 2a), even though the reactions were conducted above the temperature of H_2 recombinative desorption. In a temperature regime in which H_2 desorption does not readily occur, we expect a similar trend in H_2 production for our Pd–Au model catalysts. The 1 ML Pd–Au catalyst would have limited H_2 production due to predominantly Pd–Au interface sites but very few, if any, Pd island sites. Although the 3 and 4 ML Pd–Au catalysts would offer more EtOH activity, H_2 recombination would not occur as readily as that of the 2 ML Pd–Au catalyst, limiting H_2 production. Here, we see that our DFT calculations provide mechanistic insight for EtOH dehydrogenation and strategy for catalytic design to enhance efficiency.

It is worthwhile to note the binding configuration of the EtOH species used in our DFT calculations on the Pd ensembles, which is not always clear in the literature. Using DFT calculations, Tereshchuk et al. showed that EtOH lies down on many transition metals, including Pd(111) and Au(111), where the C–C bond is parallel with the catalytic surface.[22] For all calculations presented in Fig. 5b, EtOH has a similar lay-down orientation on all three surfaces, suggesting that Pd incorporation into the Au(111) slab does not cause a difference in adsorption orientation. Therefore, the activation energy barriers calculated are not influenced by differences in adsorption orientation on the Pd/Au(111) alloys.

Stability tests

A change in H_2 production with time would indicate a lack of stability of the Pd–Au catalysts. To further investigate the
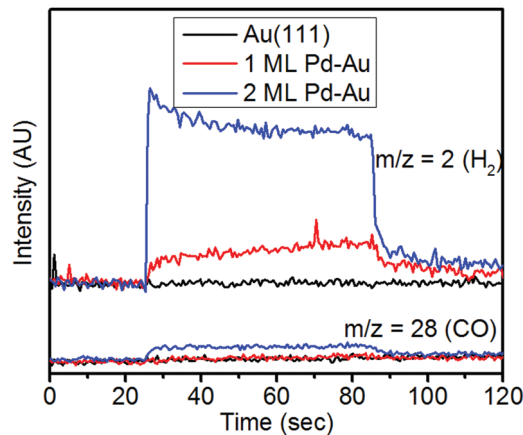

Fig. 6 H_2 and CO production from EtOH dehydrogenation on Au(111), 1 ML Pd–Au, and 2 ML Pd–Au.

stability between 1 ML and 2 ML Pd–Au catalysts, we impinged EtOH on Au(111), 1 ML Pd–Au, and 2 ML Pd–Au for 60 seconds (25–85 seconds in Fig. 6) while acquiring spectra for H_2 and CO. For the 1 ML Pd–Au catalyst, there is a constant amount of H_2 production (the increasing baseline is due to the increasing quantity of EtOH in the chamber) with no CO production, as seen in Fig. 2a. For the 2 ML Pd–Au catalyst, both CO and H_2 is produced, also seen in Fig. 2a. However, there is a continual decrease in the H_2 production while EtOH is being impinged on the surface. This change in production showcases a lack of stability for EtOH dehydrogenation for the 2 ML Pd–Au model catalyst and is indicative of a change in the catalyst that was not shown for the 1 ML Pd–Au model catalyst. This decrease in H_2 production could be due to carbon contamination blocking potential active sites. Based on our DFT calculations for Pd_4/Au(111) in Fig. 5, dehydrogenation from the β-carbon is likely on the 2 ML Pd–Au surface and the most likely pathway that would result in carbon contamination instead of the production of other small hydrocarbons. With the CH_2CH_2OH intermediate and the difficulty of cleaving the C–O bond on Pd surfaces, which would yield ethylene in this case, contamination via carbon species is a likely outcome. Also, carbon contamination can occur from reaction-limited H_2 production in which the methyl group further decomposes into carbon and H_2, as suggested on Pd(111).[29] Both pathways could result in initially blocking sites until the catalyst becomes stable, leading to the decrease in H_2 production seen in Fig. 6.

To confirm carbon contamination, we used Auger Electron Spectroscopy (AES) for elemental identification, shown in Fig. S12 of the ESI† to see the changes in the peak-to-peak ratios of Pd between a clean 2 ML Pd–Au surface and one that was exposed to EtOH impingement at 500 K for 60 s. Making a ratio using the peak-to-peak signal of the Pd feature (277 eV) that dwarfs the carbon signal (273 eV) with a peak-to-peak signal that is only determined by Pd (328 eV) can confirm the presence of carbon on a tested surface. The peak-to-peak ratio of the two Pd features for clean 2 ML Pd–Au was 4.0, but it decreased to 3.3 for the surface exposed to EtOH. This shows

that the carbon feature became more pronounced after EtOH exposure on 2 ML Pd–Au and is most likely due to carbon contamination from EtOH decomposition. However, there was no significant difference in between the Pd features of clean 1 ML Pd–Au and that of the 1 ML Pd–Au catalyst exposed to EtOH for 60 s at 500 K. Considering the DFT calculations yielding CH_2CH_2OH as a potential intermediate for the 2 ML Pd–Au catalyst, AES showing carbon contamination, and the decreasing H_2 production over 60 seconds, we believe EtOH decomposition is occurring along with EtOH dehydrogenation on the 2 ML Pd–Au catalyst, resulting in carbon species that affect the catalyst's stability at higher Pd coverages.

Additionally, we notice that the 2 ML Pd–Au catalyst has higher activity for EtOH dehydrogenation while 1 ML Pd–Au provides better stability. This interplay of stability and activity has been seen before on Pd–Au catalysts. More specifically, Xu *et al.* showed that Pd electrocatalysts with higher Au content have more stability than pure Pd on a carbon support for ethanol oxidation.[65] On the other end, pure Pd showed the highest activity with an overall decreasing trend with increasing amounts of Au incorporation. Most significantly, intermediate amounts of Pd (Pd_3Au/C) showed the greatest interplay of stability and activity. This may very well be the case with the 2 ML Pd–Au catalyst, where it is showing the highest activity for dehydrogenation with a loss of activity at the beginning of the experiment but stabilizing in activity as the experiment progresses over the 30 second impingement period.

Desorption at 77 K

To further probe the interactions of EtOH on Pd–Au surfaces, approximately 1 monolayer of EtOH was exposed to the Au(111), 1 ML Pd–Au, and 2 ML Pd–Au surfaces at 77 K. Following exposure, the sample was heated at 1 K s^{-1} to monitor EtOH desorption as shown in the TPD spectra in Fig. 7. On Au(111), EtOH does not react and desorbs at 176 K. Gong *et al.* observed desorption of EtOH on Au(111) at ~180 K and saw no products to indicate reactivity on the surface.[21] However, for 1 ML and 2 ML Pd–Au, the area under the EtOH desorption feature decreases by 3% and 8% compared to Au(111), respectively, indicating EtOH reactions on the surface as the sample is heated. Additionally, there is the appearance of a 2nd lower temperature feature, which could be due to two effects: (1) EtOH interactions on the Pd–Au surface may be such that a monolayer feature is saturated sooner or (2) decomposition of EtOH on the surface may allow other EtOH molecules to desorb more readily at lower temperatures. This second scenario is more likely considering that some EtOH reacts on the Pd–Au surface and the alkyl chains provide repulsion. The EtOH monolayer features also go to increasingly higher temperatures, supporting the fact that EtOH has a stronger interaction with Pd than Au.

In addition to adsorbing EtOH on Au(111), 1 ML Pd–Au and 2 ML Pd–Au, we also conducted DFT calculations on the binding energies of EtOH, its primary dehydrogenation product – acetaldehyde – and its three potential dehydrogenation intermediates on Pd/Au(111) with varying Pd ensembles sizes, as shown in Fig. 8. For all the species, the binding gets stronger when going from Au(111) (represented here with 0 Pd atoms), to a Pd monolayer. In particular, the strengthening of the EtOH binding energy with larger Pd ensemble sizes supports what is shown experimentally in Fig. 7, where the desorption temperature of the monolayer feature increases with increasing Pd coverage, with EtOH desorbing at 176 K, 187 K, and 196 K on Au(111), 1 ML Pd–Au and 2 ML Pd–Au, respectively. Additionally, EtOH desorbs at 200 K[29] from Pd(111) and at 247 K[28] from Pd(110), reinforcing the trend of increasing EtOH desorption temperature with increasing Pd coverage and showing how the Pd ensembles resemble the Pd(111) surface.

Furthermore, we acknowledge the large disparity in binding energies of EtOH and acetaldehyde compared to the dehydrogenation intermediates. Unless the intermediates can form acetaldehyde or other stable small molecule, the strong binding energies of the intermediates show the potential for further decomposition and catalyst contamination. The binding energies calculated for the various EtOH species provide support for the increase in desorption temperature seen in Fig. 7,
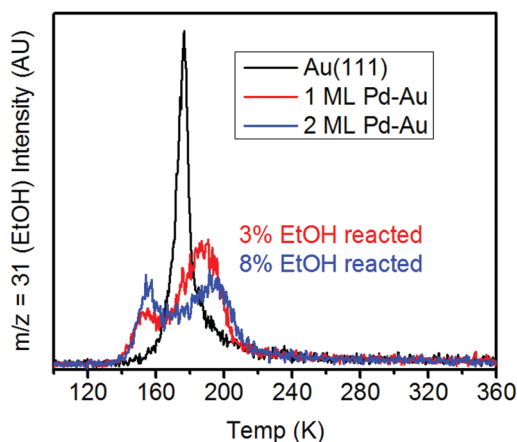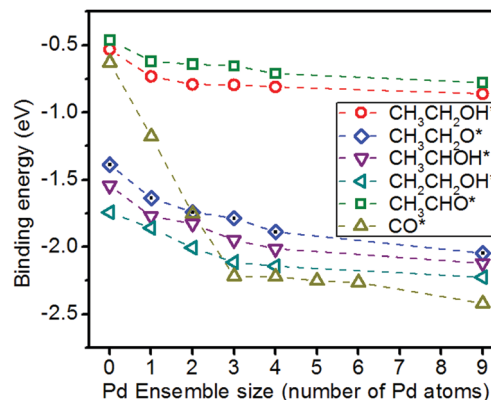

Fig. 7 TPD spectra of 1.00 ML EtOH (m/z = 31) on Au(111), 1 ML Pd–Au, and 2 ML Pd–Au adsorbed at 77 K, showcasing the difference in affinity to the model catalyst surfaces.

Fig. 8 DFT-calculated binding energies of EtOH, EtOH's three potential dehydrogenation intermediates, acetaldehyde, and CO on Pd/Au(111) with varying Pd ensemble sizes (shown in Fig. S3, ESI†).

while showing the susceptibility for intermediates to contaminate the surface.

Additionally, the binding energies of CO with varying Pd ensembles on a Au(111) slab were also calculated using DFT. CO poisoning is a major problem for fuel cell technology and very well plays a role in EtOH decomposition. Similarly to EtOH and its partially dehydrogenated intermediates, CO adsorption is stronger with larger Pd ensembles. Considering CO desorbs at 50 K on Au(111)[66] and desorbs at about 500 K on Pd(111),[67] the increase of CO binding energy with Pd is expected. In fact, Sellidj et al. saw an increase in desorption temperature in TPD with increasing Pd coverage on the Au(111) substrate, ranging from 125 K with lower Pd coverage to 500 K with multiple Pd overlayers.[68] This also supports our speculation that CO poisoning from EtOH decomposition occurs on the 2 ML Pd–Au surface and blocks H_2 evolution, as observed in our modified King and Wells experiments used to create the Arrhenius plots of Fig. 4.

Conclusions

With the synergistic effect between Pd and Au, Pd–Au bimetallics are of significant interest for many reactions and applications. In this study, we used UHV surface chemistry measurements and support from DFT calculations to investigate ethanol (EtOH) dehydrogenation on Pd–Au model catalysts. With EtOH reactive molecular beam scattering (RMBS) experiments, EtOH temperature-programmed desorption (TPD), and DFT, we show how a difference in Pd ensemble size and Pd coverage, and consequently Pd active site, on Au(111) can affect the H_2 production and the mechanism for EtOH dehydrogenation. With the catalyst held at 500 K, the 2 ML Pd–Au surface had the highest H_2 yield, outperforming catalysts with both less Pd and more Pd on their surfaces. Additionally, higher Pd coverages showed less selectivity producing CO as well as H_2 and acetaldehyde, whereas no CO was detected on 1 ML Pd–Au surfaces. Using RMBS experiments from 400–500 K, Arrhenius plots of H_2 production confirm that the reaction mechanisms for EtOH dehydrogenation differed on 1 ML Pd–Au and 2 ML Pd–Au. This supports our idea that isolated Pd atoms and Pd(111)-like sites provide different mechanisms for EtOH dehydrogenation. Using DFT, the activation barriers were calculated for the initial EtOH dehydrogenation step to support the idea of multiple reaction pathways for Pd–Au alloys. The initial dehydrogenation step depends on the size of the Pd ensemble on the Au(111) slab: based off the lowest activation barriers, Pd_1, Pd_4, and Pd_9 ensembles favor α-carbon, β-carbon, and hydroxyl dehydrogenation, respectively. RMBS experiments regarding the stability of H_2 production provide evidence of less stability on the 2 ML Pd–Au surface than the 1 ML Pd–Au surface despite the higher H_2 production on the 2 ML Pd–Au catalyst. AES suggests that carbon contamination is a contributor to this lack of stability. Using DFT binding energies and EtOH TPD, we confirm that EtOH has an increasing surface affinity to Au(111) with increasing Pd ensemble size and Pd

coverage on the Au(111) substrate, enabling more reactivity instead of facile desorption. DFT also shows stronger binding energies for the intermediates that increase with increasing Pd ensemble size, suggesting a higher probability of reaction or contamination of these surfaces. In the future, microkinetic studies fleshing out the entire mechanism of EtOH decomposition on bimetallic and practical catalysts could prove to be insightful. Hopefully, the results of this study will assist with the design of better bimetallic catalysts, especially Pd–Au alloys, for the future and provide insight into alcohol reactions and associated applications.

Conflicts of interest

There are no conflicts to declare.

Acknowledgements

Notes and references

1 R. Ramachandran and R. K. Menon, An overview of industrial uses of hydrogen, Int. J. Hydrogen Energy, 1998, 23, 593–598.

2 P. Nikolaidis and A. Poullikkas, A comparative overview of hydrogen production processes, Renewable Sustainable Energy Rev., 2017, 67, 597–611.

3 A. Kudo and Y. Miseki, Heterogeneous photocatalyst materials for water splitting, Chem. Soc. Rev., 2009, 38, 253–278.

4 M. L. Ghirardi, A. Dubini, J. Yu and P.-C. Maness, Photobiological hydrogen-producing systems, Chem. Soc. Rev., 2009, 38, 52–61.

5 P.-Y. Sheng, G. A. Bowmaker and H. Idriss, The Reactions of Ethanol over Au/CeO2, Appl. Catal., A, 2004, 261, 171–181.

6 E. C. Wanat, K. Venkataraman and L. D. Schmidt, Steam reforming and water–gas shift of ethanol on Rh and Rh–Ce catalysts in a catalytic wall reactor, Appl. Catal., A, 2004, 276, 155–162.

7 M. A. Goula, S. K. Kontou and P. E. Tsiakaras, Hydrogen production by ethanol steam reforming over a commercial Pd/γ-Al2O3 catalyst, Appl. Catal., B, 2004, 49, 135–144.

8 G. A. Deluga, J. R. Salge, L. D. Schmidt and X. E. Verykios, Renewable Hydrogen from Ethanol by Autothermal Reforming, Science, 2004, 303, 993–997.

9 T. Hou, S. Zhang, Y. Chen, D. Wang and W. Cai, Hydrogen production from ethanol reforming: catalysts and reaction mechanism, Renewable Sustainable Energy Rev., 2015, 44, 132–148.

10 A. Haryanto, S. Fernando, N. Murali and S. Adhikari, Current Status of Hydrogen Production Techniques by Steam Reforming of Ethanol: A Review, Energy Fuels, 2005, 19, 2098–2106.

This journal is © the Owner Societies 2017

Phys. Chem. Chem. Phys., 2017, 19, 30578–30589 | 30587

11 D. K. Liguras, D. I. Kondarides and X. E. Verykios, Production of hydrogen for fuel cells by steam reforming of ethanol over supported noble metal catalysts, *Appl. Catal., B*, 2003, **43**, 345–354.

12 J. Breen, R. Burch and H. Coleman, Metal-catalysed steam reforming of ethanol in the production of hydrogen for fuel cell applications, *Appl. Catal., B*, 2002, **39**, 65–74.

13 C. Xu, L. Cheng, P. Shen and Y. Liu, Methanol and ethanol electrooxidation on Pt and Pd supported on carbon microspheres in alkaline media, *Electrochem. Commun.*, 2007, **9**, 997–1001.

14 C. Xu, P. K. Shen and Y. Liu, Ethanol electrooxidation on Pt/C and Pd/C catalysts promoted with oxide, *J. Power Sources*, 2007, **164**, 527–531.

15 L. D. Zhu, T. S. Zhao, J. B. Xu and Z. X. Liang, Preparation and characterization of carbon-supported sub-monolayer palladium decorated gold nanoparticles for the electrooxidation of ethanol in alkaline media, *J. Power Sources*, 2009, **187**, 80–84.

16 Q. He, W. Chen, S. Mukerjee, S. Chen and F. Laufek, Carbon-supported PdM (M = Au and Sn) nanocatalysts for the electrooxidation of ethanol in high pH media, *J. Power Sources*, 2009, **187**, 298–304.

17 J. B. Xu, T. S. Zhao, Y. S. Li and W. W. Yang, Synthesis and characterization of the Au-modified Pd cathode catalyst for alkaline direct ethanol fuel cells, *Int. J. Hydrogen Energy*, 2010, **35**, 9693–9700.

18 J. T. Kozlowski and R. J. Davis, Heterogeneous Catalysts for the Guerbet Coupling of Alcohols, *ACS Catal.*, 2013, **3**, 1588–1600.

19 B. Xu, R. J. Madix and C. J. Friend, Achieving Optimum Selectivity in Oxygen Assisted Alcohol Cross-Coupling on Gold, *J. Am. Chem. Soc.*, 2010, **132**, 16571–16580.

20 X. Liu, B. Xu, J. Haubrich, R. J. Madix and C. M. Friend, Surface-Mediated Self-Coupling of Ethanol on Gold, *J. Am. Chem. Soc.*, 2009, **131**, 5757–5759.

21 J. Gong and C. B. Mullins, Selective oxidation of ethanol to acetaldehyde on gold, *J. Am. Chem. Soc.*, 2008, **130**, 16458–16459.

22 P. Tereshchuk and J. L. F. Da Silva, Ethanol and Water Adsorption on Close-Packed 3d, 4d, and 5d Transition-Metal Surfaces: A Density Functional Theory Investigation with van der Waals Correction, *J. Phys. Chem. C*, 2012, **116**, 24695–24705.

23 Q. S. Meng, Y. L. Shen, J. Xu and J. L. Gong, Mechanistic Insights into Selective Oxidation of Ethanol on Au(111): A DFT Study, *Chin. J. Catal.*, 2012, **33**, 407–415.

24 B. Huang, R. Chen and Q. S. Chen, DFT Study on Effect of Hydrogen-Bond Formation on the Adsorption of Ethanol on Pd(111) Surface, *Asian J. Chem.*, 2013, **25**, 2156–2160.

25 J. L. Davis and M. A. Barteau, Spectroscopic identification of alkoxide, aldehyde, and acyl intermediates in alcohol decomposition on Pd(111), *Surf. Sci.*, 1990, **235**, 235–248.

26 M. Li, W. Guo, R. Jiang, L. Zhao and H. Shan, Decomposition of Ethanol on Pd(111): A Density Functional Theory Study, *Langmuir*, 2010, **26**, 1879–1888.

27 W. Guo, M. Li, X. Lu, H. Zhu, Y. Li, S. Li and L. Zhao, Ethanol decomposition on a Pd(110) surface: a density functional theory investigation, *Dalton Trans.*, 2013, **42**, 2309–2318.

28 R. Shekhar and M. A. Barteau, Structure sensitivity of alcohol reactions on (110) and (111) palladium surfaces, *Catal. Lett.*, 1995, **31**, 221–237.

29 J. L. Davis and M. A. Barteau, Decarbonylation and decomposition pathways of alcohol's on Pd(111), *Surf. Sci.*, 1987, **187**, 387–406.

30 B. Pawelec, A. M. Venezia, V. La Parola, E. Cano-Serrano, J. M. Campos-Martin and J. L. G. Fierro, AuPd alloy formation in Au–Pd/Al$_2$O$_3$ catalysts and its role on aromatics hydrogenation, *Appl. Surf. Sci.*, 2005, **242**, 380–391.

31 B. A. Ferguson, C. T. Reeves and C. B. Mullins, Oxygen adsorption on Si(100)-2 × 1 *via* trapping-mediated and direct mechanisms, *J. Chem. Phys.*, 1999, **110**, 11574.

32 M. C. Wheeler, D. C. Seets and C. B. Mullins, Kinetics and dynamics of the initial dissociative chemisorption of oxygen on Ru(001), *J. Chem. Phys.*, 1996, **105**, 1572.

33 B. E. Koel, A. Sellidj and M. T. Paffett, Ultrathin films of Pd on Au(111): evidence for surface alloy formation, *Phys. Rev. B: Condens. Matter Mater. Phys.*, 1992, **46**, 7846–7856.

34 G. Kresse and J. Hafner, *Ab initio* molecular dynamics for liquid metals, *Phys. Rev. B: Condens. Matter Mater. Phys.*, 1993, **47**, 558–561.

35 P. E. Blöchl, Projector augmented-wave method, *Phys. Rev. B: Condens. Matter Mater. Phys.*, 1994, **50**, 17953–17979.

36 G. Kresse and D. Joubert, From ultrasoft pseudopotentials to the projector augmented-wave method, *Phys. Rev. B: Condens. Matter Mater. Phys.*, 1999, **59**, 1758–1775.

37 J. P. Perdew, K. Burke and M. Ernzerhof, Generalized Gradient Approximation Made Simple, *Phys. Rev. Lett.*, 1996, **77**, 3865–3868.

38 P. Hohenberg and W. Kohn, Inhomogeneous Electron Gas, *Phys. Rev.*, 1964, **136**, B864–B871.

39 W. Kohn and L. J. Sham, Self-Consistent Equations Including Exchange and Correlation Effects, *Phys. Rev.*, 1965, **140**, A1133–A1138.

40 S. Grimme, J. Antony, S. Ehrlich and H. Krieg, A consistent and accurate ab initio parametrization of density functional dispersion correction (DFT-D) for the 94 elements H-Pu, *J. Chem. Phys.*, 2010, **132**, 154104.

41 H. J. Monkhorst and J. D. Pack, Special points for Brillouin-zone integrations, *Phys. Rev. B: Solid State*, 1976, **13**, 5188–5192.

42 M. Methfessel and A. T. Paxton, High-precision sampling for Brillouin-zone integration in metals, *Phys. Rev. B: Condens. Matter Mater. Phys.*, 1989, **40**, 3616–3621.

43 G. Henkelman, B. P. Uberuaga and H. Jónsson, A climbing image nudged elastic band method for finding saddle points and minimum energy paths, *J. Chem. Phys.*, 2000, **113**, 9901–9904.

44 T. Kondo, K. Tamura, M. Takahasi, J. Mizuki and K. Uosaki, A novel spectroelectrochemical cell for in situ surface X-ray scattering measurements of single crystal disk electrodes, *Electrochim. Acta*, 2002, **47**, 3075–3080.

30588 | *Phys. Chem. Chem. Phys.*, 2017, **19**, 30578–30589

This journal is © the Owner Societies 2017

45 W.-Y. Yu, L. Zhang, G. M. Mullen, G. Henkelman and C. B. Mullins, Oxygen Activation and Reaction on Pd–Au Bimetallic Surfaces, *J. Phys. Chem. C*, 2015, **119**, 11754–11762.

46 W.-Y. Yu, L. Zhang, G. M. Mullen, E. J. Evans, G. Henkelman and C. B. Mullins, Effect of annealing in oxygen on alloy structures of Pd–Au bimetallic model catalysts, *Phys. Chem. Chem. Phys.*, 2015, **17**, 20588–20596.

47 H. D. Shih, E. Bauer and H. Poppa, Low temperature alloying in the Pd/Au system, *Thin Solid Films*, 1982, **88**, L21–L24.

48 C.-W. Yi, K. Luo, T. Wei and D. W. Goodman, The Composition and Structure of Pd–Au Surfaces, *J. Phys. Chem. B*, 2005, **109**, 18535–18540.

49 W.-Y. Yu, G. M. Mullen and C. B. Mullins, Hydrogen Adsorption and Absorption with Pd–Au Bimetallic Surfaces, *J. Phys. Chem. C*, 2013, **117**, 19535–19543.

50 W.-Y. Yu, G. M. Mullen, D. W. Flaherty and C. B. Mullins, Selective hydrogen production from formic acid decomposition on Pd–Au bimetallic surfaces, *J. Am. Chem. Soc.*, 2014, **136**, 11070–11078.

51 G. E. Gdowski, T. E. Felter and R. H. Stulen, Effect of Surface Temperature on the Sorption of Hydrogen by Pd(111), *Surf. Sci.*, 1987, **181**, L147–L155.

52 N. Takehiro, P. Liu, A. Bergbreiter, J. K. Nørskov and R. J. Behm, Hydrogen adsorption on bimetallic PdAu(111) surface alloys: minimum adsorption ensemble, ligand and ensemble effects, and ensemble confinement, *Phys. Chem. Chem. Phys.*, 2014, **16**, 23930–23943.

53 R. J. Behm, K. Christmann and G. Ertl, Adsorption of hydrogen on Pd(100), *Surf. Sci.*, 1980, **99**, 320–340.

54 R. J. Behm, V. Penka, M. G. Cattania, K. Christmann and G. Ertl, Evidence for '''subsurface''' hydrogen on Pd(110): an intermediate between chemisorbed and dissolved species, *J. Chem. Phys.*, 1983, **78**, 7486.

55 P. Kunal, H. Li, B. L. Dewing, L. Zhang, K. Jarvis, G. Henkelman and S. M. Humphrey, Microwave-Assisted Synthesis of Pd$_x$Au$_{100-x}$ Alloy Nanoparticles: a Combined Experimental and Theoretical Assessment of Synthetic and Compositional Effects upon Catalytic Reactivity, *ACS Catal.*, 2016, **6**, 4882–4893.

56 L. Luo, Z. Duan, H. Li, J. Kim, G. Henkelman and R. M. Crooks, Tunability of the Adsorbate Binding on Bimetallic Alloy Nanoparticles for the Optimization of Catalytic Hydrogenation, *J. Am. Chem. Soc.*, 2017, **139**, 5538–5546.

57 C. M. Moore, O. Staples, R. W. Jenkins, T. J. Brooks, T. A. Semelsberger, A. D. Sutton, J. G. Linger, E. M. Karp, D. Salvachúa, D. R. Vardon and G. T. Beckham, Acetaldehyde as an ethanol derived bio-building block: an alternative to Guerbet chemistry, *Green Chem.*, 2017, **19**, 169–174.

58 W.-Y. Yu, G. M. Mullen and C. B. Mullins, Interactions of Hydrogen and Carbon Monoxide on Pd–Au Bimetallic Surfaces, *J. Phys. Chem. C*, 2014, **118**, 2129–2137.

59 R. M. Williams, S. H. Pang and J. W. Medlin, OH versus CH bond scission sequence in ethanol decomposition on Pd(111), *Surf. Sci.*, 2014, **619**, 114–118.

60 H. C. Ham, J. A. Stephens, G. S. Hwang, J. Han, S. W. Nam and T. H. Lim, Pd ensemble effects on oxygen hydrogenation in AuPd alloys: a combined density functional theory and Monte Carlo study, *Catal. Today*, 2011, **165**, 138–144.

61 P. Liu and J. K. Nørskov, Ligand and ensemble effects in adsorption on alloy surfaces, *Phys. Chem. Chem. Phys.*, 2001, **3**, 3814–3818.

62 D. W. Yuan and Z. R. Liu, Atomic ensemble effects on formic acid oxidation on PdAu electrode studied by first-principles calculations, *J. Power Sources*, 2013, **224**, 241–249.

63 B. Coq and F. Figueras, Bimetallic palladium catalysts: influence of the co-metal on the catalyst performance, *J. Mol. Catal. A: Chem.*, 2001, **173**, 117–134.

64 W. P. Zhou, A. Lewera, R. Larsen, R. I. Masel, P. S. Bagus and A. Wieckowski, Size Effects in Electronic and Catalytic Properties of Unsupported Palladium Nanoparticles in Electrooxidation of Formic Acid, *J. Phys. Chem. B*, 2006, **110**, 13393–13398.

65 J. B. Xu, T. S. Zhao, S. Y. Shen and Y. S. Li, Stabilization of the palladium electrocatalyst with alloyed gold for ethanol oxidation, *Int. J. Hydrogen Energy*, 2010, **35**, 6490–6500.

66 D. P. Engelhart, R. J. V. Wagner, A. Meling, A. M. Wodtke and T. Schäfer, Temperature programmed desorption of weakly bound adsorbates on Au(111), *Surf. Sci.*, 2016, **650**, 11–16.

67 X. Guo and J. T. Yates, Dependence of effective desorption kinetic parameters on surface coverage and adsorption temperature: CO on Pd(111), *J. Chem. Phys.*, 1989, **90**, 6761.

68 A. Sellidj and B. E. Koel, Electronic and CO chemisorption properties of ultrathin Pd films vapor deposited on Au(111), *Phys. Rev. B: Condens. Matter Mater. Phys.*, 1994, **49**, 8367–8376.